Reinforcing multiwall carbon nanotubes by electron beam irradiation

Martial Duchamp,[1] Richard Meunier,[1] Rita Smajda,[1] Marijana Mionic,[1] Arnaud Magrez,[1,2] Jin Won Seo,[3] László Forró,[1] Bo Song,[4] and David Tománek[5,6,a)]

[1]*Laboratoire de Nanostructures et Nouveaux Matériaux Electroniques (LNNME), Ecole Polytechnique Fédérale de Lausanne (EPFL), 1015 Lausanne, Switzerland*
[2]*Center for Research on Electronically Advanced Materials, Ecole Polytechnique Fédérale de Lausanne (EPFL), 1015 Lausanne, Switzerland*
[3]*Department of Metallurgy and Materials Engineering, Katholieke Universiteit Leuven, Kasteelpark Arenberg 44, 3001 Heverlee, Belgium*
[4]*Shanghai Institute of Applied Physics, Chinese Academy of Sciences, P.O. Box 800-204, Shanghai 201800, China*
[5]*Centre Européen de Calcul Atomique et Moléculaire (CECAM), Ecole Polytechnique Fédérale de Lausanne (EPFL), 1015 Lausanne, Switzerland*
[6]*Department of Physics and Astronomy, Michigan State University, East Lansing, Michigan 48824-2320, USA*

We study the effect of electron beam irradiation on the bending modulus of multiwall carbon nanotubes grown by chemical vapor deposition. Atomic force microscopy observations of the nanotube deflection in the suspended-beam geometry suggest an internal, reversible stick-slip motion prior to irradiation, indicating presence of extended defects. Upon electron beam irradiation, nanotubes with an initial bending modulus exceeding 10 GPa initially get stiffer, before softening at high doses. Highly defective nanotubes with smaller initial bending moduli do not exhibit the initial reinforcement. These data are explained by *ab initio* molecular dynamics calculations suggesting a spontaneous cross-linking of neighboring nanotube walls at extended vacancy defects created by the electron beam, in agreement with electron microscopy observations. At low defect concentration, depending on the edge morphology, the covalent bonds between neighboring nanotube walls cause reinforcement by resisting relative motion of neighboring walls. At high concentration of defects that are present initially or induced by high electron beam dose, the structural integrity of the entire system suffers from increasing electron beam damage. © *2010 American Institute of Physics.* [doi:10.1063/1.3493049]

Exceptionally high elastic modulus and tensile strength count among the most prominent properties of carbon nanotubes,[1] lending themselves to a wide range of applications. Theoretical studies[2,3] predict unprecedented values of 1 TPa for the Young's modulus and 100 GPa for the tensile strength of defect free single wall carbon nanotubes (SWNTs). These theoretical predictions have been confirmed in particular for the outer walls of multiwall carbon nanotubes (MWNTs) produced by arc discharge (AD).[4] Whereas mechanical properties of single-wall and double-wall nanotubes are usually very favorable independent of the production process,[5] nanotubes with many walls display a poorer mechanical performance.[6] Among those, MWNTs produced by the low-cost chemical vapor deposition (CVD) process in presence of a catalyst have substantially poorer mechanical properties than arc-grown nanotubes. Electron beam irradiation has been shown to induce cross-linking between bundled SWNTs (Ref. 7) and between adjacent walls of AD grown MWNTs.[4] This morphology change has the potential to significantly suppressed relative slippage of walls,[8] which is responsible also for the low shear modulus of graphite. In bundles of SWNTs (Ref. 7) and in arc-grown MWNTs,[4] electron beam irradiation has increased the stiffness and maxi-

mum load by one order of magnitude with respect to the as-grown samples.

We focus in the following on the mechanical properties of CVD-grown MWNTs, which form the bulk fraction of mass-produced carbon nanotubes. In spite of significant improvements in the growth process, these nanotubes contain many defects that deteriorate their mechanical properties and limit their application range. Depending of the kind and density of defects, the measured bending modulus E_b ranges from 1 GPa to 1 TPa (Ref. 9) and the tensile strength covers the range from 20 to 260 GPa.[10] This unusually large variation in the mechanical properties of CVD-MWNTs differentiates these nanotubes significantly from AD-MWNTs studied in Ref. 4 and has been linked structurally to high-quality segments that are joined by poor-quality nodes[9] in the wall structure, as shown schematically in Fig. 1(e).

Here we report the results of a combined experimental and theoretical study of the effect of electron-beam irradiation on the mechanical properties of CVD-grown MWNTs. Our experimental results are obtained for individual nanotubes with initial bending moduli E_b ranging between 3 GPa and 1 TPa, which have been exposed to various levels of electron irradiation. We find a strong correlation between the diameter, structural perfection and elastic properties of MWNTs. The initial bending modulus of narrow nanotubes

---

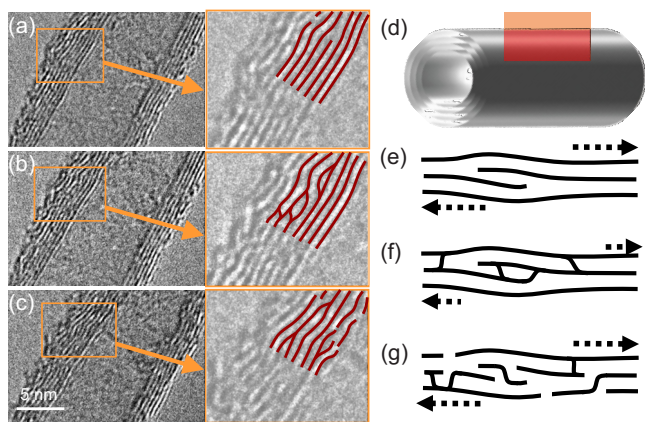a)Electronic mail: tomanek@pa.msu.edu.

FIG. 1. (Color online) Structural changes in MWNTs subject to electron beam irradiation. High-resolution transmission electron micrographs of MWNTs exposed to a current density of 4.76×10^{19} e/(cm² s) during (a) 24 s, (b) 49 s, and (c) 3 min 44 s. Dark lines in the enlarged segments of the micrographs on the right indicate the position of walls. The effect of electron irradiation within the wall region, indicated in (d), is shown schematically in (e)–(g). (e) Presence of large scale defects in multiwall nanotubes reduces significantly the Young's and the shear modulus, resulting in large displacements in response to shear stress. (f) The main effect of electron beam irradiation is to create vacancy defects in adjacent walls that spontaneously cross-link adjacent walls, thus increasing the bending modulus and reducing the shear motion in response to shear stress. (g) Defect percolation in nanotubes of either initial poor quality or tubes subject to excessive irradiation continues to lower the bending modulus upon additional irradiation. Displacement in response to shear stress increases in this case.

with diameters $d \leq 12$ nm is very high and experiences only moderate improvement upon irradiation cross-linking between walls. Wider nanotubes in the diameter range 12 nm $\leq d \leq 25$ nm show a significant improvement of their bending modulus upon irradiation for the same reason. Very wide nanotubes with $d \geq 30$ nm carry initially a high density of defects. In this case, introduction of additional defects by irradiation causes an overall weakening of the structure despite cross-linking. Using *ab initio* molecular dynamics (MD) simulations, we show that cross-linking of neighboring walls is a spontaneous process occurring only at pristine vacancy defect edges facing each other, as produced by energetic electrons. No such cross-linking occurs when defect edges do not face each other or are chemically passivated, as confirmed by the observed absence of structural reinforcement in case of thermal annealing only.

In this study we use two types of CVD-grown carbon nanotubes. We grow wide nanotubes with an outer diameter larger than 20 nm using acetylene on a CaCO₃ supported Fe₂Co alloy catalyst[11] and narrower nanotubes in the diameter range 8 nm $\leq d \leq 16$ nm using ethylene on alumina supported Fe catalyst in presence of water.[12] The sample preparation and experimental details are described in the Ref. 13. Detailed structural investigation of the nanotubes has been performed using a high-resolution transmission electron microscope (HRTEM) operating at 200 keV. HRTEM images of a typical as-grown nanotube subject to increasing levels of irradiation are shown in Figs. 1(a)–1(c). The dynamics of the structural changes during irradiation can be viewed in the movie contained in Ref. 13. Schematic images of possible native or irradiation-induced defects, as well as expected strain following axial stress, are illustrated in Figs. 1(d)–1(g).

Isolated nanotubes have been mounted on microfabricated Si₃N₄ membranes with predrilled 200 nm to 1 μm wide holes. This substrate is suitable for both mechanical measurements and direct observation by electron microscopy. Nanotube alignment and deposition across the holes was assisted by a dielectrophoretic set-up with metal electrodes.[14] The mechanical properties of the mounted nanotubes have been probed by an atomic force microscope (AFM) in the geometry depicted in Fig. 2(a). The nanotubes have then been subject to an electron beam irradiation in a scanning TEM (STEM) operating at 200 kV. Since we chose the outer dimensions of the nanotube support to fit both the TEM and AFM sample holders, this set-up allowed for bending modulus measurement and electron irradiation on the same, individual carbon nanotube. We consider this capability a significant improvement over the results presented in Ref. 4 that are based on additional assumptions due to the inability to correlate structural and mechanical changes in individual nanotubes. To establish a dependable correlation between the electron dose and elastic properties, we performed AFM measurements at different stages of irradiation. The electron irradiation dose was determined with no sample in the beam, by taking the ratio of the average current and the exposed area.

Initial measurements of the suspended length and diameter of the nanotubes were performed using both the STEM and AFM. Mechanical properties have been determined by recording the deflection $\delta z(x)$ of the AFM tip at a fixed position x along the suspended nanotube as a function of the applied load, which was successively increased and decreased. As we describe later on, the recorded AFM data allowed us to deduce the bending modulus E_b in the elastic regime.

The following results of our bending test provide a more detailed insight into the correlation between specific defects and the elastic behavior than the traction test used in Ref. 4, which averages out important microscopic effects. Figure 2(c) displays the deflection profile $\delta z(x)$ of a $d=20$ nm wide nanotube prior to and following an electron beam irradiation dose of 2×10^{19} e/cm² under different loads. Subjecting the as-grown nanotube to a constant load $F = 20$ nN, δz exhibits several plateaus arranged in terraces. Our interpretation in terms of a relative stick-slip motion of neighboring walls at defect sites is illustrated in the inset of Fig. 2(c). The rather smooth polynomial profile, expected for a double-clamped beam,[15] and the significantly lower deflection $\delta z(x)$ observed under an even higher load $F = 32$ nN, suggest that this treatment has suppressed the effect of structural inhomogeneities on the elastic behavior of the nanotube. Such structural inhomogeneities in the as-grown nanotubes are attributed to their structure,[9] consisting of high-quality segments linked by soft nodes. The exact nature of these nodes may vary from tube to tube. HRTEM observations suggest that these nodes may be associated with weak interactions between walls of rigid cones or cups in cup-stacked tubes, bamboo nodes in bamboolike nanotubes, and incomplete nanotube walls in CVD-grown MWNTs.[9]

As indicated in the schematic Fig. 2(b), bending of nanotubes with many walls and a large diameter involves both
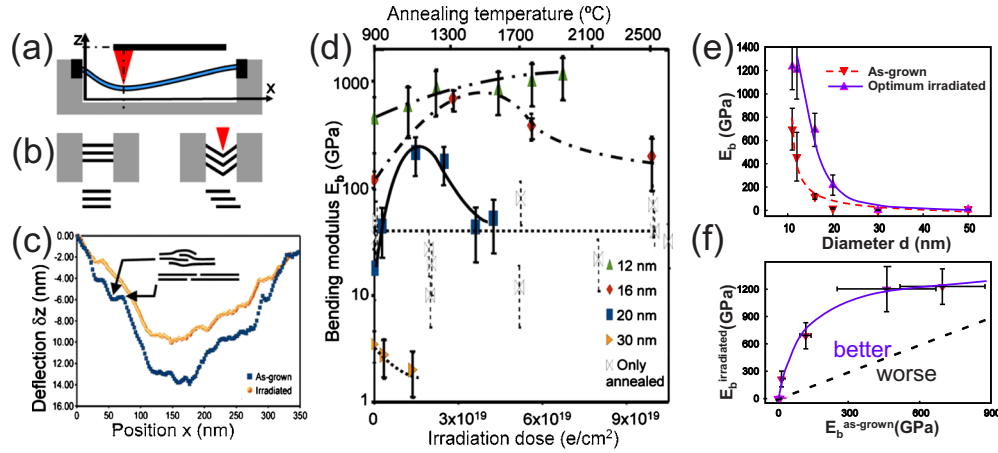
FIG. 2. (Color online) Elastic properties of MWNTs subject to heat treatment or electron beam irradiation. (a) AFM setup to measure the deflection δz of a suspended nanotube as a function of the tip position x. The nanotube is suspended over a trench and anchored at both ends. (b) Illustration of the fact that in response to the force exerted by the AFM tip the deformation of ideally clamped nanotubes with many walls involves both stretch and shear. (c) AFM measurement of the deflection profile $\delta z(x)$ of a 20 nm wide carbon nanotube, suspended across a 350 nm wide trench. The deflection of the nanotube in response to a loading force $F=20$ nN exerted by the AFM tip, labeled "as-grown" and depicted by the dark data points (■), is rather large and exhibits plateaus due to stick-slip motion, as illustrated in the inset. Following irradiation with the optimal dose 2×10^{19} e/cm², these plateaus are suppressed and the deflection is reduced when the tube is subject to an even larger loading force $F=32$ nN, as shown by the light data points (●). (d) Observed dependence of the bending modulus E_b of various carbon nanotubes on tube treatment. In absence of electron irradiation, annealing in the temperature range between $900-2500$ °C, labeled on the upper abscissa, does not change the bending modulus of nanotubes with $d=10-15$ nm within the error bars of the observation in Ref. 17; this is depicted by the dotted line as a guide to the eye connecting the data points (◄►). Unlike annealing only, electron beam irradiation does cause significant changes in the bending modulus of multi-wall nanotubes. For the sake of consistency, we performed AFM measurements on the same nanotube exposed to a varying degree of electron irradiation. As-grown nanotubes with $E_b > 10$ GPa display an initial E_b enhancement upon moderate irradiation, which reverts to a gradual decrease in E_b beyond an optimum irradiation dose. No initial E_b enhancement is observed in nanotubes with low initial bending modulus $E_b < 10$ GPa, as shown by the data points (►). (e) Dependence of E_b on the diameter of as-grown and irradiated nanotubes. (f) Comparison between E_b in as-grown and irradiated nanotubes. Results for irradiated nanotubes in (e) and (f) refer to the irradiation dose that maximizes structural reinforcement.

stretch and shear motion of the coaxial walls. Consequently, the observed deflection $\delta z(x)$ of a MWNT clamped on both ends in response to the force F applied by the AFM tip depends not only on the Young's modulus E but also the shear modulus G. The general expression for any position x is quite complex but simplifies for the mid-beam position to[16]

$$\delta z(L/2) = \frac{FL^3}{192EI} + f_s \frac{FL}{4GA} = \frac{FL^3}{192E_bI}. \quad (1)$$

Here L is the total length of the nanotube in suspension, I is the second moment of the nanotube cross-section, and f_s is the shape factor that equals 10/9 for a cylindrical beam. According to Eq. (1), the bending modulus E_b could be considered an "effective Young's modulus if shear were of no concern."

The observed dependence of the bending modulus E_b of MWNTs with different diameters on the electron irradiation dose and annealing temperature is presented in Fig. 2(d). The data cover nanotubes with diameters ranging from 12–30 nm and E_b values of as-grown samples ranging from 20 GPa to 1 TPa. Our results indicate the possibility to distinguish between two types of nanotubes. Whereas E_b is observed to increase following initial irradiation in *Type I* nanotubes, E_b only decreases in *Type II* nanotubes following any irradiation. This rich behavior is in stark contrast with the monotonous degradation of AD-MWNTs by irradiation, reported in Ref. 4. In contrast to irradiation, thermal annealing in the temperature range between $900-2500$ °C does not change the bending modulus of nanotubes with $d=10-15$ nm

within the error bars of the observation in Ref. 17 that are also shown in Fig. 2(d).

Our results in Fig. 2(d) indicate that as-grown *Type I* nanotubes are characterized by a narrow diameter not exceeding ≈ 20 nm and a large value E_b in excess of ≈ 10 GPa. The initially increasing E_b reaches a maximum before starting to decrease following an optimum irradiation dose in all *Type I* nanotubes. *Type II* nanotubes, according to Fig. 2(d), are characterized by a wide diameter exceeding ≈ 20 nm and a low value E_b below ≈ 10 GPa. The essence of our mechanical measurements for as-grown nanotubes and nanotubes subject to the optimum irradiation dose for structural reinforcement is summarized in Figs. 2(e) and 2(f). The rapid deterioration of the bending modulus with increasing nanotube diameter is shown in Fig. 2(e). These results clearly show that significant increase in the bending modulus E_b upon irradiation only occurs in rather narrow high-quality nanotubes with a large enough initial value $E_b > 10$ GPa. The same results are presented in a different way in Fig. 2(f) that shows the maximum achievable improvement of the bending modulus of as-grown nanotubes by irradiation.

As we discuss in the following, this observed mechanical behavior can be traced back to variations in defect morphology and concentration, and to the effect of electron irradiation on both. We notice that the initial increase and subsequent decrease of E_b in *Type I* nanotubes is more dramatic among the wider nanotubes with a low initial bending modulus. These systems are close to or beyond the rigidity percolation limit in the sense that at least a fraction of the MWNT constituents are rigidly connected, forming a percolation path of covalent bonds between the nanotube ends. We

believe that the initial enhancement in E_b upon irradiation is caused by cross-linking adjacent wall segments by covalent bonds, as illustrated by the change in the wall structure in Fig. 1(e) to that in Fig. 1(f). We notice that the optimum dose for optimum structural reinforcement, ranging between $\approx 1 \times 10^{19} - 5 \times 10^{19}$ e/cm^2, increases with decreasing diameter and increasing initial E_b value in *Type I* tubes. This range of irradiation doses had also been shown to cause cross-linking among the 2–5 outermost walls in AD grown MWNTs (Ref. 4) and between SWNTs in bundles.[7] Obviously, the strain in response to the same axial stress should decrease during such a process, as indicated by the length change in the dashed arrows in Figs. 1(e) and 1(f). In fact, as seen in Fig. 2(d), this cross-linking of the outermost walls suppresses slippage in our *Type I* CVD-grown nanotubes, hence increasing the shear modulus G and thus E_b by up to a factor of five.

The eventual decrease in E_b at irradiation doses beyond the optimum value can be traced back to a very high density of irradiation-induced defects that eventually destroy the rigidity percolation path in the graphitic nanotube walls, as shown schematically in Fig. 1(g). This conclusion agrees with the observation that high doses of 200 kV TEM irradiation create stable vacancies in double-wall nanotubes.[18]

Theoretical studies of the effect of irradiation-induced vacancy defects on the elastic properties of free-standing high-quality nanotubes[4,19,20] indicate that the Young's modulus of these systems may decrease by only $\approx 3\%$ even at rather high vacancy concentrations. Results of total energy[19,20] and MD (Ref. 21) calculations witness an unusual capability of nanotubes to heal these defects by reconstructing at vacancy sites. In the CVD grown carbon nanotubes considered here, the wide range of the observed Young's moduli as well as the HRTEM images of tube morphology presented in Fig. 1 indicate a strong adverse effect of defects on the elastic behavior of as-grown nanotubes and suggest that the most common defects are not pointlike but rather extended. Even though reconstruction at dislocation lines connecting a scroll with a nanotube[22] and at unterminated double-wall nanotube edges[23] have been found energetically favorable, those theoretical results refer to specific cases that may not resemble the processes in the systems studied here.

To better understand the effect of irradiation on the mechanical properties of CVD-grown nanotubes, we performed MD simulations of the reconstruction process. Since the semiempirical Tersoff–Brenner functional used in Ref. 4 does not reliably describe complex formation and breaking of bonds, we rather used an *ab initio* approach and based our total energy and force calculations on the density functional theory (DFT).[24] We used the Perdew–Zunger[25] form of the exchange-correlation functional in the local density approximation[26] to DFT, as implemented in the SIESTA code with local orbitals.[27] The behavior of valence electrons was described by norm-conserving Troullier–Martins pseudopotentials[28] and a double-zeta basis.

Since we are particularly interested in the reconstruction at extended defect sites, we selected a graphene bilayer with zigzag (ZZ) and armchair (AC) edges as a model system. For the sake of convenience when using periodic boundary conditions, we considered infinitely long bilayer strips with a
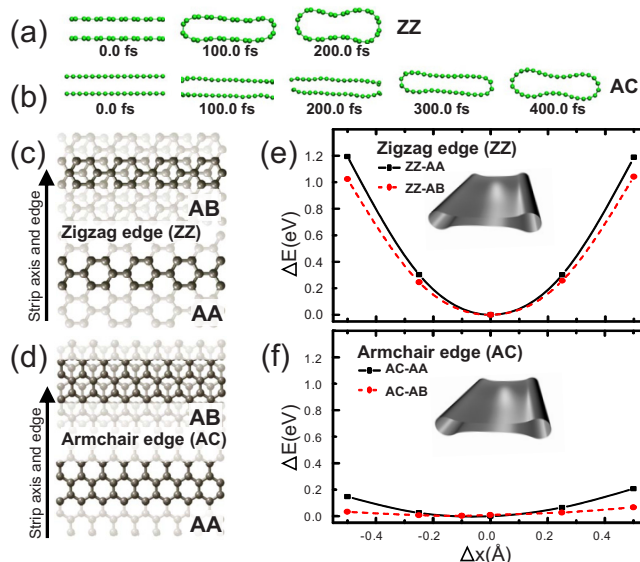

FIG. 3. (Color online) Results of *ab initio* MD simulations of cross-link formation and structural reinforcement at exposed edges of an extended vacancy defect, modeled by a narrow bilayer graphene strip. The cross-linking dynamics, shown by a sequence of snap shots depicting spontaneous formation of bonds connecting the edges of a graphene bilayer with (a) ZZ and (b) AC edges at $T=800$ K. (c) Morphology of a ZZ graphene bilayer strip with AA and AB layer stacking in top view. (d) Morphology of an AC graphene bilayer strip with AA and AB layer stacking in top view. The bottom layer is shown by a lighter color than the top layer, and the size the unit cell is further enhanced by the darker color in (c) and (d). Energy cost ΔE to displace the topmost layer by Δx in the direction of the edge per 1 nm length of one edge in cross-linked (e) ZZ and (f) AC bilayer strips. We find $\Delta E \approx 0$ in all cases when the layers are not cross-linked.

finite width, shown in Fig. 3. Unlike in as-grown CVD nanotubes, where vacancy defects with unsaturated edges seldom face each other in adjacent walls, exactly such defects are expected to form as a result of energetic irradiation by electrons, justifying our choice of the model geometry. In view of the fact that the chiral indices in neighboring nanotube walls may not be related, we considered two different initial layer registries, namely the AB stacking found in hexagonal graphite and the AA stacking with the strips initially on top of each other. The unit cells for the different edge and stacking geometries in the infinite strip are shown in top view in Figs. 3(c) and 3(d) and in side view as the leftmost frames of Figs. 3(a) and 3(b).

The reaction dynamics of carbon nanotubes during e-beam irradiation is very complex, as it involves electronic excitations moving the system off the Born–Oppenheimer surface. To account for the effect of irradiation we considered an effective temperature above the vacancy migration temperature in graphene (500 K) and layered BN (800 K).[29] We performed MD simulations of the canonical ensemble (with constant number of particles N, volume V and temperature T) consisting of the unit cell of AB and AA stacked layers with ZZ and AC edges using a Nosé–Hoover thermostat that kept the average temperature at $T=800$ K. We used periodic boundary conditions and kept the graphitic strips in neighboring unit cells at least 7 Å apart to suppress spurious interactions. Our time step of 0.3 fs was found adequate to reproduce the proper dynamics by keeping the total energy conserved in a separate microcanonical MD calculation.

Results of our MD simulations are illustrated as snap shots in Figs. 3(a) and 3(b), and as movies in the associated Ref. 13. We found that independent of the initial stacking, all unsaturated edges in the bilayer formed covalent cross-links on a time scale ranging from 0.2–0.4 ps. This is a very fast process that would even compete successfully with edge functionalization under different conditions during nanotube growth in presence of carbon feedstock.[23] The higher reactivity of the ZZ edge as compared to the AC edge, caused by its higher edge energy, translates to a larger energy gain associated with cross-linking adjacent edges. The corresponding energy gain per nanometer length of the ZZ edge is 23.6 eV (ZZ-AA) and 21.5 eV (ZZ-AB), much higher than the values 8.8 eV (AC-AA) and 4.2 eV (AC-AB) per nanometer length of the AC edge. The morphology of the ZZ-terminated graphene bilayer allows a covalent connection between its components to a strained but defect-free sp^2 network with a much larger energy gain than found at the AC edge. This higher energy gain associated with cross-linking ZZ edges in comparison to AC edges is also responsible for reducing the cross-linking time by one half with respect to the AC edge, as seen in Figs. 3(a) and 3(b).

Finally, we discuss the effect of cross-linking at extended defects on the elastic properties. As a basis for our reasoning, we consider a pair of aligned unterminated edges in adjacent layers of a MWNT caused by irradiation. Cross-linking in the way discussed above connects the adjacent walls covalently, whereby initial ZZ edges are expected to form the strongest bonds. We expect the shear modulus and thus the bending modulus of such a tube to increase especially if the defect edge is almost parallel to the tube axis. In this configuration, which does not cause contrast changes in HRTEM images, shear of neighboring walls translates to a relative displacement Δx of adjacent, connected edges in the direction of the edge. As shown in Figs. 3(e) and 3(f), a significant energy penalty, comparable to the bond strength, is associated with this local shear. This energy penalty is particularly high in the case of a ZZ-edge vacancy defect, where the rigidity of the inter-layer bond is related to the (in-plane) shear resistance of an individual graphene monolayer. The enhancement of the shear modulus by forming covalent bonds among initially disconnected layers is responsible for the initial increase in the shear and thus the bending modulus of lightly defective *Type I* nanotubes, displayed in Fig. 2. Since the discussed mechanism is only active at sites with matching unterminated edge pairs, which are missing in as-grown nanotubes, we expect and observe no reinforcement by annealing only. Such unterminated edge pairs, however, which are capable of providing reinforcement, may be created by electron beam irradiation. Obviously, no amount of irradiation may provide any reinforcement for initially highly defective *Type II* nanotubes with a high concentration of disconnected wall segments. Finally, very high irradiation doses cause more structural damage than reinforcement and thus lead to an eventual decrease in the bending modulus in any nanotube.

In conclusion, we studied the effect of electron beam irradiation on the bending modulus of MWNTs grown by CVD, which dominate the nanotube market for applications.

Our AFM observations of the nanotube deflection in the suspended-beam geometry suggest an internal, reversible stick-slip motion prior to irradiation, indicating presence of extended defects. Upon electron beam irradiation, we found that nanotubes with an initial bending modulus exceeding 10 GPa get stiffer by up to a factor of five initially and subsequently soften at higher doses. Highly defective nanotubes with smaller initial bending moduli do not exhibit such initial reinforcement. Our observations are explained by *ab initio* MD calculations suggesting a spontaneous cross-linking of neighboring nanotube walls at extended vacancy defects created by the electron beam, in agreement with electron microscopy observations. At low defect concentration, depending on the edge morphology, the covalent bonds between neighboring nanotube walls cause reinforcement by resisting relative slip motion of neighboring walls. At high concentrations of defects that are present initially or induced by high electron beam dose, the structural integrity of the entire system suffers from increasing electron beam damage. Our results suggest that electron irradiation is a useful tool to improve the elastic properties even of defective MWNTs produced in large quantities by CVD synthesis.

[1] A. Jorio, M. Dresselhaus, and G. Dresselhaus, *Carbon Nanotubes: Advanced Topics in the Synthesis, Structure, Properties and Applications*, Topics in Applied Physics Vol. 111 (Springer, New York, 2008).

[2] G. Overney, W. Zhong, and D. Tománek, Z. Phys. D: At., Mol. Clusters **27**, 93 (1993).

[3] S. Ogata and Y. Shibutani, Phys. Rev. B **68**, 165409 (2003).

[4] B. Peng, M. Locascio, P. Zapol, S. Li, S. Mielke, G. Schatz, and H. Espinosa, Nat. Nanotechnol. **3**, 626 (2008).

[5] Y. Wu, M. Huang, F. Wang, X. M. H. Huang, S. Rosenblatt, L. Huang, H. Yan, S. P. O'Brien, J. Hone, and T. Heinz, Nano Lett. **8**, 4158 (2008).

[6] B. Lukić, J. W. Seo, R. R. Bacsa, S. Delpeux, F. Béguin, G. Bister, A. Fonseca, J. B. Nagy, A. Kis, S. Jeney, A. J. Kulik, and L. Forró, Nano Lett. **5**, 2074 (2005).

[7] A. Kis, G. Csanyi, J. Salvetat, T. Lee, E. Couteau, A. Kulik, W. Benoit, J. Brugger, and L. Forró, Nature Mater. **3**, 153 (2004).

[8] S. Cui, I. A. Kinloch, R. J. Young, L. Noe, and M. Monthioux, Adv. Mater. **21**, 3591 (2009).

[9] K. Lee, B. Lukic, A. Magrez, J. Seo, G. Briggs, A. Kulik, and L. Forró, Nano Lett. **7**, 1598 (2007).

[10] A. Barber, I. Kaplan-Ashiri, S. Cohen, R. Tenne, and H. Wagner, Compos. Sci. Technol. **65**, 2380 (2005).

[11] A. Magrez, J. W. Seo, V. L. Kuznetsov, and L. Forró, Angew. Chem., Int. Ed. **46**, 441 (2007).

[12]R. Smajda, J. C. Andresen, M. Duchamp, M. Meunier, S. Casimirius, K. Hernádi, L. Forró, and A. Magrez, Phys. Status Solidi B **246**, 2457 (2009).

[13]See supplementary material at http://dx.doi.org/10.1063/1.3493049 for details of sample preparation and instrumentation as well as links to movies depicting the MD simulations.

[14]M. Duchamp, K. Lee, B. Dwir, J. W. Seo, E. Kapon, L. Forró, and A. Magrez, ASC Nano **4**, 279 (2010).

[15]W. Mai and Z. L. Wang, Appl. Phys. Lett. **89**, 073112 (2006).

[16]J.-P. Salvetat, G. Briggs, D. Andrew, J-M. Bonard, R. Bacsa, A. Kulik, T. Stöckli, N. Burnham, and L. Forró, Phys. Rev. Lett. **82**, 944 (1999).

[17]B. Lukic, J. W. Seo, E. Couteau, K. Lee, S. Gradecak, R. Berkecz, K. Hernadi, S. Delpeux, T. Cacciaguerra, F. Beguin, A. Fonseca, J. B. Nagy, G. Csanyi, A. Kis, A. J. Kulik, and L. Forró, Appl. Phys. A: Mater. Sci. Process. **80**, 695 (2005).

[18]J. Rodriguez-Manzo and F. Banhart, Nano Lett. **9**, 2285 (2009).

[19]M. Sammalkorpi, A. Krasheninnikov, A. Kuronen, K. Nordlund, and K. Kaski, Phys. Rev. B **70**, 245416 (2004); **71**, 169906(E) (2005).

[20]M. Huhtala, A. Krasheninnikov, J. Aittoniemi, K. Nordlund, S. J. Stuart, and K. Kaski, Phys. Rev. B **70**, 045404 (2004).

[21]Y. Miyamoto, S. Berber, M. Yoon, A. Rubio, and D. Tománek, Physica B **323**, 78 (2002).

[22]J. G. Lavin, S. Subramoney, R. S. Ruoff, S. Berber, and D. Tománek, Carbon **40**, 1123 (2002).

[23]Y.-K. Kwon, Y. H. Lee, S.-G. Kim, P. Jund, D. Tománek, and R. E. Smalley, Phys. Rev. Lett. **79**, 2065 (1997).

[24]P. Hohenberg and W. Kohn, Phys. Rev. **136**, B864 (1964).

[25]J. P. Perdew and A. Zunger, Phys. Rev. B **23**, 5048 (1981).

[26]W. Kohn and L. Sham, Phys. Rev. **140**, A1133 (1965).

[27]J. M. Soler, E. Artacho, J. D. Gale, A. García, J. Junquera, P. Ordejón, and D. Sánchez-Portal, J. Phys.: Condens. Matter **14**, 2745 (2002).

[28]N. Troullier and J. L. Martins, Phys. Rev. B **43**, 1993 (1991).

[29]A. Zobelli, A. Gloter, C. P. Ewels, and C. Colliex, Phys. Rev. B **77**, 045410 (2008).